Testing the high turbulence level breakdown of low-frequency gyrokinetics against high-frequency cyclokinetic simulationsa)

Zhao Deng and R. E. Waltz

Testing the high turbulence level breakdown of low-frequency gyrokinetics against high-frequency cyclokinetic simulations[a)]

Zhao Deng[1,b),c)] and R. E. Waltz[2]

[1]*State Key Laboratory of Nuclear Physics and Technology, School of Physics, Peking University, Beijing 100871, China*
[2]*General Atomics, P.O. Box 85608, San Diego, California 92186-5608, USA*

This paper presents numerical simulations of the nonlinear cyclokinetic equations in the cyclotron harmonic representation [R. E. Waltz and Zhao Deng, Phys. Plasmas **20**, 012507 (2013)]. Simulations are done with a local flux-tube geometry and with the parallel motion and variation suppressed using a newly developed rCYCLO code. Cyclokinetic simulations dynamically follow the high-frequency ion gyro-phase motion which is nonlinearly coupled into the low-frequency drift-waves possibly interrupting and suppressing gyro-averaging and increasing the transport over gyrokinetic levels. By comparing the more fundamental cyclokinetic simulations with the corresponding gyrokinetic simulations, the breakdown of gyrokinetics at high turbulence levels is quantitatively tested over a range of relative ion cyclotron frequency $10 < \Omega^* < 100$ where $\Omega^* = 1/\rho^*$, and ρ^* is the relative ion gyroradius. The gyrokinetic linear mode rates closely match the cyclokinetic low-frequency rates for $\Omega^* > 5$. Gyrokinetic transport recovers cyclokinetic transport at high relative ion cyclotron frequency ($\Omega^* \geq 50$) and low turbulence level as required. Cyclokinetic transport is found to be lower than gyrokinetic transport at high turbulence levels and low-Ω^* values with stable ion cyclotron (IC) modes. The gyrokinetic approximation is found to break down when the density perturbations exceed 20%. For cyclokinetic simulations with sufficiently unstable IC modes and sufficiently low $\Omega^* \sim 10$, the high-frequency component of cyclokinetic transport level can exceed the gyrokinetic transport level. However, the low-frequency component of the cyclokinetic transport and turbulence level does not exceed that of gyrokinetics. At higher and more physically relevant $\Omega^* \geq 50$ values and physically realistic IC driving rates, the low-frequency component of the cyclokinetic transport and turbulence level is still smaller than that of gyrokinetics. Thus, the cyclokinetic simulations do not account for the so-called "L-mode near edge short fall" seen in some low-frequency gyrokinetic transport and turbulence simulations. © 2015 AIP Publishing LLC. [http://dx.doi.org/10.1063/1.4917176]

I. INTRODUCTION AND SUMMARY

Gyrokinetic simulations of some near edge L-mode tokamak plasmas with the GYRO code[1] have been found to under predict both the transport and the turbulence levels by at least 5-fold[2] or even 10-fold in the more turbulent and colder edge.[3] This missing transport and low-frequency turbulence (so called "L-mode near edge short-fall") suggest that either some important mechanism is missing from current gyrokinetic codes like GYRO, or the gyrokinetic approximation itself is breaking down. This paper tests for the high turbulence level breakdown of low-frequency gyrokinetics against high-frequency nonlinear cyclokinetic[4] simulations. Cyclokinetic simulations dynamically follow the high-frequency ion gyro-phase motion and nonlinearly couple the high-frequency ion cyclotron modes to the low-frequency drift modes. Gyrokinetics is an approximation of cyclokinetics obtained by gyro-averaging over the high-frequency gyro-motion in cyclokinetics. The linear low-frequency drift mode rates in cyclokinetics and gyrokinetics

are the same. Nonlinear cyclokinetics has no limit on the amplitude of the perturbations, whereas gyrokinetics is limited to the low drift-wave frequencies much less than the ion cyclotron frequencies and weak turbulence levels (with the perturbed $E \times B$ velocity much less than the ion thermal velocity $\delta v_\perp^E \ll v_i^{th}$ on the small scale of the ion gyroradius $(\rho k_\perp) \sim O(1)$ in Ref. 5, p. 113, where k is the wave number). It is known that GYRO drift-kinetic ion simulations with gyro-averaging suppressed can recover most of the missing transport.[3] The high-frequency gyro-motion included in cyclokinetics possibly interrupts and suppresses the gyro-averaging if the turbulence level is high enough. It is also possible that sufficiently unstable high-frequency ion cyclotron modes could nonlinearly drive low-frequency turbulence and transport. This leads us to conjecture that the low-frequency component of cyclokinetic transport level might be driven higher than gyrokinetics so as to recover the L-mode near edge "short-fall."

With these motivations, a 4D [k_x, k_y, μ, α] reduced nonlinear cyclokinetic[4] code rCYCLO was developed. k_x, k_y are the wave-number Fourier transform of the cross-field space positions x, y. μ is magnetic moment, and α is the ion gyrophase. The 2D [k_z, v_z] parallel motion is suppressed for

---

simplicity. By comparing the 4D [k_x, k_y, μ, α] rCYCLO cyclokinetic transport simulations with the correspondingly 3D [k_x, k_y, μ] gyrokinetic transport simulations, we can quantitatively test the breakdown of gyrokinetics and gyro-averaging at high enough turbulence level and low enough relative ion cyclotron frequency Ω^*, where $\Omega^* = 1/\rho^*$ and ρ^* is the relative ion gyroradius. rCYCLO dynamically follows the high-frequency ion gyro-motion with no averaging over the gyro-phase α. There is no approximation in the $E \times B$ nonlinearity. Only the electrostatic perturbations in a local flux-tube geometry are considered, with a shearless B-field decreasing in the radial x direction. This produces a y directed grad-B drift. The simulation box (or local flux-tube cross section) size is much larger than the eddy size (typically tens of ion gyro-radii) and much smaller than the variations in the gradient lengths, which are typically close to the machine minor radius size. The ion density and temperature gradients are fixed. The electrons are treated with a collisional drift wave (CDW) and resistive-g mode fluid model. The rCYCLO code nonlinearly couples the toroidally (grad-B) driven ion temperature gradient (ITG) modes and the CDW modes to the ion cyclotron (IC) modes.

The purpose of this work is to investigate the effect of the nonlinear coupling between the high-frequency ion cyclotron motion and low-frequency drift motion. Therefore, it is important that no approximation on the cross-field nonlinear $E \times B$ motion is made. What kind of mode is linearly driven unstable or what artificial damping is chosen is less important, as long as the same model is used in both cyclokinetics and gyrokinetics. The model gyrokinetic linear rates must match the model cyclokinetic low-frequency linear rates. The parallel nonlinearity is one order smaller than the cross-field $E \times B$ nonlinearity since $k_\parallel/k_\perp = 1/\Omega^*$. Gyrokinetic codes typically omit the parallel nonlinearity. The trapped particle modes and the Landau damping in the parallel direction are not relevant to the breakdown of gyrokinetics. Thus, we omit the parallel motion and parallel variations in rCYCLO.

Cyclokinetics in the gyro-phase angle form and cyclokinetics in cyclotron harmonic form (CKinCH) were given in Ref. 4. The numerical methods for nonlinear simulations of cyclokinetics in the gyro-phase Fourier harmonic form (CKinFH) were detailed in Ref. 6, where the grid convergences for the rCYCLO code were also demonstrated. Only the CKinCH form is used for nonlinear cyclokinetic simulations in this work. The magnetic moment μ-grids, the corresponding velocity space μ-weights, and the numerical treatment of the μ-derivative operator (which enters the $E \times B$ nonlinearity) are carefully chosen to nonlinearly conserve the incremental entropy of the turbulence. An implicit time linear advance step followed by a lag time nonlinear step is applied. The numerical treatments for CKinFH in Ref. 6 remain unchanged for CKinCH in this work. Nonlinear CKinCH simulations are more expensive than CKinFH simulations, but the CKinCH formulation is more transparently related to gyrokinetics.

The numerical simulations of CKinCH with rCYCLO in this work have recovered the simulations of CKinFH in Ref. 6 which were limited to stable high-frequency ion cyclotron modes. At sufficiently large relative cyclotron frequency ($\Omega^* > 5$), gyrokinetic recovers the low-frequency linear growth rates and frequencies in either form of cyclokinetics. At sufficiently large $\Omega^* \geq 50$ and sufficiently low turbulence level, the nonlinear gyrokinetic simulations have recovered the cyclokinetic transport levels as required. In the cyclokinetic simulations, we found that (1) the transport level of cyclokinetics with stable IC modes is lower, not higher, than the gyrokinetic transport at low $\Omega^* \sim 10$ values; (2) gyrokinetics starts to break down when turbulence level $|\delta n/n_0|$ exceeds 20%. Physically relevant values of Ω^* are in the range of 50–100. The turbulence is drained in frequency space from the unstable low-frequency domain and spreads into the less unstable high-frequency domain. The transport level of cyclokinetics is lower than that of gyrokinetics, because the turbulence is drained to the less unstable IC modes. The breakdown of the gyrokinetic gyroBohm to Bohm scaling by draining and spreading in frequency space at small Ω^* is analogous to the breakdown of gyroBohm to Bohm scaling by draining and spreading in real space at large ρ^* found in the gyrokinetic nonlocal simulations.[7,8] It is reasonable to ask if the direction of draining and spreading from low to high frequency can be reversed with highly unstable IC modes, then the cyclokinetic low-frequency transport might be driven higher than gyrokinetics. We found that with sufficiently unstable IC modes, the high-frequency component of cyclokinetic transport level can exceed the gyrokinetic transport level at sufficient low $\Omega^* \sim 10$, and the direction of draining and spreading can be reversed. However, in these simulations, the low-frequency component of the cyclokinetic transport and turbulence level did not exceed that of gyrokinetics. At higher and more physically relevant $\Omega^* \geq 50$ values with physically realistic IC driving rates, the low-frequency component of the cyclokinetic transport still cannot be driven higher than gyrokinetics. Thus, the L-mode near edge "short-fall" is not due to the nonlinear coupling between low-frequency drift motion and high-frequency ion cyclotron motion.

While highly driven IC mode simulations may not be physically relevant, they were found to provide a perhaps unique example of bifurcated turbulent transport states. When the maximum high-frequency (HF) driving rate is about twice the maximum low-frequency (LF) driving rate, a HF low transport level state can "jump" to a LF high transport level state. These HF and LF transport states represent two "basins" of nonlinear saturation. The corresponding electrostatic energy also saturates into two bifurcated steady states but without a jump in the total: the electrostatic energy is simply redistributed from low-frequency modes to high-frequency modes.

The remainder of the paper is structured as follows. Formulations of ion cyclokinetics, ion gyrokinetics, and electron dynamics are given in Sec. II. The nonlinear simulations of CKinCH are presented in Sec. III, where the simulations of CKinCH are shown to recover the simulations of CKinFH with stable IC modes.[6] New simulations with unstable IC modes are presented. Conclusions are given in Sec. IV.

II. FORMULATIONS

A. Cyclokinetic equations in gyro-phase angle form

Starting with the six-dimensional collisionless Vlasov-Poisson equations, rCYCLO assumes a two-dimensional local flux-tube geometry (x, y) perpendicular to magnetic field $\vec{B}$. Parallel variations and parallel velocity are suppressed $\partial/\partial_z \Rightarrow 0$, $u_z \Rightarrow 0$. The simulation box (x, y) is a small symmetric rectangle of side L with $\rho_s \ll L \ll a$. ρ_s is the ion gyro-radius, and a is the tokamak minor radius. The straight and shearless magnetic field varies only in the x direction $B(x) = B[1 - (x + r)/R]$. x represents the radial position with $x = 0$ at center of the box, R is the tokamak major radius, and r is the minor radius of the flux tube. Since no trapped particles are considered, the value of the local inverse aspect ratio r/R does not enter in this work. rCYCLO transforms real space (x, y) to Fourier wave-number space (k_x, k_y). Following from Eq. (9b) of Ref. 4, the nonlinear non-conservative form of the normalized ion cyclokinetic equation in gyro-phase angle space is given by

$$D\delta\hat{f}_k/D\hat{t} - i\hat{\omega}_k^d \delta\hat{g}_k + i\vec{v}_\perp \cdot \vec{k}\Omega_* \delta\hat{g}_k - \Omega_* \partial_\alpha \delta\hat{g}_k$$
$$= -i\hat{\omega}_{*k}^{nT}\delta\hat{\phi}_k n_0 F_M(\hat{\mu})$$
$$+ \sum_{k1}[(T_e/T_i)\delta\hat{\phi}_{k1}i\vec{k}_1 \cdot \vec{v}_\perp \partial_{\hat{\mu}}\delta\hat{f}_{k2}$$
$$+ \delta\hat{\phi}_{k1}i\vec{k}_1 \cdot \hat{b} \times \vec{v}_\perp/\hat{v}_\perp^2 \partial_\alpha \delta\hat{f}_{k2}], \qquad (1)$$

where $\delta\hat{\phi}_k$ is the perturbed electric potential, $\delta\hat{f}_k$ is the perturbed ion distribution function and $\delta\hat{g}_k(\hat{\mu}, \alpha) = \delta\hat{f}_k(\hat{\mu}, \alpha) + (T_e/T_i)\delta\hat{\phi}_k n_0 F_M(\hat{\mu})$ represents the non-adiabatic part of the distribution function. α is the gyro-phase angle. $\mu = m_i v_\perp^2/2B$ is the ion magnetic moment with the perpendicular ion velocity $v_\perp$ and the ion mass m_i. T_e (T_i) is the electron (ion) temperature, n_0 is the unperturbed ion density, and $F_M(\hat{\mu})$ is the two-dimensional Maxwell ion distribution function. In rCYCLO, variables are normalized to gyroBohm units. Macro-lengths are scaled to the tokamak minor radius a, cross-field micro-turbulence lengths to the sound speed ion gyro-radius ρ_s, velocities to the ion sound speed c_s, time to a/c_s, and ion velocity to the ion thermal speed $v_i^{th} = \sqrt{2T_i/m_i}$. The ion sound speed is defined by $c_s = \sqrt{T_e/m_i}$, with $\rho_s = c_s/\Omega$ where $\Omega = eB/m_i c$ is the ion gyro frequency. $\vec{k}_\perp = k_\perp[\cos(\beta)\hat{\varepsilon}_x + \sin(\beta)\hat{\varepsilon}_y]$ is the cross-field wave-number vector in Cartesian coordinates with $\hat{\varepsilon}_y = \hat{\varepsilon}_z \times \hat{\varepsilon}_x$, $\hat{\varepsilon}_z = \hat{b} = \vec{B}/B$, and β is the wave angle. Replace $k_\perp$ with k for convenience, since all wave-number vectors are in cross-field plane. The three-wave interaction requires $\vec{k}_2 = \vec{k} - \vec{k}_1$. The perpendicular ion velocity can be expressed as $\vec{v}_\perp = v_\perp(\hat{\varepsilon}_x \cos\alpha + \hat{\varepsilon}_y \sin\alpha)$ with $0 \le \alpha < 2\pi$. We normalize the wave number, time, and magnetic moment as $\hat{k} = k_\perp \rho_s$, $\hat{t} = t(c_s/a)$, and $\hat{\mu} = (v_\perp/v_i^{th})^2$, respectively. The perturbed ion distribution function, electric potential, and Maxwell distribution function are normalized as $\delta\hat{f}_k = (\delta f_k T_i/m_i)/\rho^*$, $\delta\hat{\phi}_k = (e\delta\phi_k/T_e)/\rho^*$, and $F_M(\hat{\mu}) = e^{-\hat{\mu}}/2\pi$, respectively, where $\rho^* = \rho_s/a$ is the relative ion gyro radius. $\hat{\omega}_k^d = 2\hat{k}_y(T_i/T_e)\hat{\mu}(a/R)$ is the grad-B

drift frequency. We have added the factor 2 here to compensate for the curvature drive from the suppressed parallel direction. $\hat{\omega}_*^{nT} = \hat{k}_y[(a/L_n) + (a/L_{Ti})(\hat{\mu} - 1)]$ is the density and temperature gradient drive frequency for the drift waves. In rCYCLO, artificial damping at high and low k is built into time derivative operator $D/D\hat{t} = \partial/\partial\hat{t} + \mu_{HK}\hat{k}^4 + \mu_{LK}/\hat{k}^2$. μ_{HK} and μ_{LK} are constants. $\mu_{HK}\hat{k}^4$ represents the damping of high-k modes which allows turbulence energy to escape to short wave-length modes where it is physically damped by collisions. $\mu_{LK}/\hat{k}^2$ is the damping of low-k modes. It physically represents the neglected magnetic shear damping which makes the low-k modes slightly stable. This allows the low-k modes to saturate the inverse cascade energy from the higher k driving modes. The large factor $\Omega^* = 1/\rho^*$ is the relative ion cyclotron frequency, which ranges from 10 to 1000 with 50 to 100 being the typically physical values of interest. We set $n_0 \equiv 1$ in units of density n_e, which means $n_i = n_e$. The velocity space integration of the two-dimensional Maxwell ion distribution function is $\oint d\alpha \int_0^\infty d\hat{\mu}F_M(\hat{\mu}) = 1$ where the parallel velocity has been suppressed. The perturbed potential and distribution function satisfy the reality condition $\delta\hat{\phi}_{-k} = \delta\hat{\phi}_k^*$, $\delta\hat{f}_{-k} = \delta\hat{f}_k^*$. Note that cyclokinetics does not assume $\delta f/F \ll 1$, where F is the equilibrium background distribution.

The Poisson equation is given as

$$(\hat{\lambda}_D^2 \hat{k}^2)\delta\hat{\phi}_k = \oint d\alpha \int_0^\infty d\hat{\mu}\delta\hat{f}_k(\hat{\mu}, \alpha)/n_0 - \delta\hat{n}_k^e, \qquad (2)$$

where $\hat{\lambda}_D \ll 1$ is the Debye length in units of ρ_s. $\delta\hat{n}_k^e = (\delta n_k^e/n_0)/\rho^*$ is the normalized perturbed electron density, and $\delta\hat{n}_k^i = \oint d\alpha \int_0^\infty d\hat{\mu}\delta\hat{f}_k(\hat{\mu}, \alpha)/n_0$ is the normalized perturbed ion density. The electron equations of motion are given in Sec. II D.

The radial ion particle and energy fluxes in gyroBohm units of $n_0 c_s \rho^{*2}$ and $T_e n_0 c_s \rho^{*2}$ are

$$[\hat{\Gamma}, \hat{Q}^\perp] = \mathrm{Re}\oint d\alpha \int_0^\infty d\hat{\mu}\sum_k[1, (T_i/T_e)\hat{\mu}]i\hat{k}_y\delta\hat{\phi}_k^*[\delta\hat{g}_k(\hat{\mu}, \alpha)/n_0],$$
$$(3)$$

where Re means only the real part is retained. $\delta\hat{g}_k$ indicates that transport is proportional to the non-adiabatic perturbed distribution function. The diffusivities are defined as fluxes divided by gradients $[\hat{D}, \hat{\chi}] = [\hat{\Gamma}, \hat{Q}^\perp]/[a/L_n, a/L_{Ti}]$.

We do not attempt to simulate Eq. (1) since the stiff α-derivative term $\Omega_* \partial_\alpha \delta\hat{g}_k$ is difficult to time advance accurately. It is better to transform α to a harmonic space so as to replace the derivative operator by the harmonic number identity $\partial_\alpha \Rightarrow in$. There are two kinds of harmonic transforms: Fourier harmonics and cyclotron harmonics. Nonlinear CKinFH simulations were presented in Ref. 6, where the numerical methods were documented and grid convergences were demonstrated. The formulation of CKinFH is given in the Appendix. The simulations in this paper were done in the CKinCH representation to which we now turn.

B. Cyclokinetic equations in cyclotron harmonic form

For the convenience of the readers, we follow Ref. 4 to provide the nonlinear cyclokinetic equations in cyclotron harmonic form (CKinCH). The cyclotron harmonic transform is defined by

$$\delta \hat{f}_k(\hat{\mu}, \alpha) \exp[-ik\rho \sin(\alpha - \beta)]$$
$$= \sum_{n=-N_\alpha+1}^{n=N_\alpha-1} \delta \hat{F}_k^n(\hat{\mu}) \exp[in(\alpha - \beta)], \qquad (4)$$

where $\rho = v_\perp/\Omega$ is ion gyro radius. [The Eq. (12) of Ref. 4 used $ik\rho \sin(\alpha - \beta)$, when it should have been $-ik\rho \sin(\alpha - \beta)$.] In order to formulate numerically practical equations, we apply finite expansion in gyro-phase space here instead of infinite expansion in Ref. 4. $n = -N_\alpha$ $+1, \ldots 0 \ldots, N_\alpha - 1$ is the harmonic number with respect to α. Unlike the Fourier harmonics, the cyclotron harmonics are the linearly uncoupled "normal modes" of cyclokinetics. The CKinCH nonlinear simulations are considerably more expensive than the CKinFH, but CKinCH is more easily identified with gyrokinetics analytically.

Equation (1) is in non-conservative form, and we can obtain its conservative form by applying the crucial identity Eq. (5) to its nonlinear term

$$(T_e/T_i)\partial_{\hat{\mu}}\vec{\hat{k}}_1 \cdot \vec{\hat{v}}_\perp + \partial_\alpha\vec{\hat{k}}_1 \cdot \hat{b} \times \vec{\hat{v}}_\perp/\hat{v}_\perp^2 = 0. \qquad (5)$$

Applying the cyclotron harmonic transform Eq. (4) to Eq. (1), we obtain the non-conservative nonlinear expression of CKinCH, which is given as

$$D\delta\hat{F}_k^n/D\hat{t} - i\hat{\omega}_k^d\delta\hat{G}_k^n - in\Omega_*\delta\hat{G}_k^n + J_n(k\rho)\delta\hat{\phi}_k i\hat{\omega}_{*k}^{nT}n_0 F_M(\hat{\mu})$$
$$= \sum_{n'}\sum_{k1} \hat{b} \cdot \vec{\hat{k}}_1 \times \vec{\hat{k}}_2 [J_{n-n'}(k_1\rho)]\delta\hat{\phi}_{k1}\delta\hat{F}_{k2}^{n'}\Delta_n^{n'}(\beta, \beta_1, \beta_2)$$
$$+ \sum_{n'}\sum_{k1} (\hat{k}_1/\hat{v}_\perp)\{[J_{n-n'+1}(k_1\rho) - J_{n-n'-1}(k_1\rho)]/(2i)\}\delta\hat{\phi}_{k1}(n'\delta\hat{F}_{k2}^{n'})\Delta_n^{n'}(\beta, \beta_1, \beta_2)$$
$$+ \sum_{n'}\sum_{k1} (\hat{k}_1/\hat{v}_\perp)\{[J_{n-n'+1}(k_1\rho) + J_{n-n'-1}(k_1\rho)]/(2i)\}\delta\hat{\phi}_{k1}(2\hat{\mu}\partial_{\hat{\mu}}\delta\hat{F}_{k2}^{n'})\Delta_n^{n'}(\beta, \beta_1, \beta_2). \qquad (6)$$

CKinCH with the conservative nonlinear expression is written compactly as

$$D\delta\hat{F}_k^n/D\hat{t} - i\hat{\omega}_k^d\delta\hat{G}_k^n - in\Omega_*\delta\hat{G}_k^n + J_n(k\rho)\delta\hat{\phi}_k i\hat{\omega}_{*k}^{nT}n_0 F_M(\hat{\mu})$$
$$= \sum_{n'}\sum_{k1} \hat{b} \cdot \vec{\hat{k}}_1 \times \vec{\hat{k}}_2 [J_{n-n'}(k_1\rho)]\delta\hat{\phi}_{k1}\delta\hat{F}_{k2}^{n'}\Delta_n^{n'}(\beta, \beta_1, \beta_2)$$
$$+ \sum_{n'}\sum_{k1} (\hat{k}_1/\hat{v}_\perp)\{[J_{n-n'+1}(k_1\rho) - J_{n-n'-1}(k_1\rho)]/(2i)\}\delta\hat{\phi}_{k1}(n\delta\hat{F}_{k2}^{n'})\Delta_n^{n'}(\beta, \beta_1, \beta_2)$$
$$+ \sum_{n'}\sum_{k1} \delta\hat{\phi}_{k1}(T_e/T_i)\partial_{\hat{\mu}}\{[J_{n-n'+1}(k_1\rho) + J_{n-n'-1}(k_1\rho)](\hat{k}_1\hat{v}_\perp)\delta\hat{F}_{k2}^{n'}/(2i)\}\Delta_n^{n'}(\beta, \beta_1, \beta_2). \qquad (7)$$

$\delta\hat{F}_k^n(\hat{\mu}) = \delta\hat{G}_k^n(\hat{\mu}) - J_n(k\rho)\delta\hat{\phi}_k(T_e/T_i)n_0 F_M(\hat{\mu})$, and $J_n(k_1\rho)$ is Bessel function. $\Delta_n^{n'}(\beta, \beta_1, \beta_2) \equiv \exp[-in(\beta_1 - \beta)$ $+in'(\beta_1 - \beta_2)]$ is a phase factor between different wave angles. $\sum_{n'}$ represents $\sum_{n'=-N_\alpha+1}^{n'=N_\alpha-1}$. The perturbed distribution function satisfies the reality condition $\delta\hat{F}_{-k}^{-n} = (-1)^n[\delta\hat{F}_k^n]^*$. After some careful algebra, the conservative and non-conservative forms are found to be equivalent as required. Notice that the nonlinear coupling coefficient in the last two lines of nonlinear term is enhanced by $1/\hat{v}_\perp$ at low velocities.

In rCYCLO code, the nonlinear term is calculated by adding the conservative form with the equivalent non-conservative form of nonlinear terms and divided by 2. This operation cancels any numerical errors from the μ-derivative operator (described in Ref. 6) in the nonlinear conservation of incremental entropy. The incremental entropy of CKinCH is defined by

$$S = \sum_k \oint d\alpha \int_0^\infty d\hat{\mu}(\delta\hat{f}_k^*\delta\hat{f}_k) = 2\pi \int_0^\infty d\hat{\mu}\sum_k\sum_n(\delta\hat{F}_k^n)^*\delta\hat{F}_k^n. \qquad (8)$$

Using the conservative nonlinear expression Eq. (7) together with the non-conservative expression Eq. (6), it is straightforward to prove CKinCH nonlinear entropy conservation. Numerical nonlinear incremental entropy conservation is a crucial test of any turbulence simulation code (e.g., see Ref. 9 in the case of the GYRO code). The discretization of the derivative operator $\partial_{\hat{\mu}}$ is designed to ensure the conservation of the incremental entropy as discussed in Ref. 6.

The Poisson equation for CKinCH is given as

$$\delta\hat{\phi}_k = \frac{\sum_n 2\pi \int d\hat{\mu}J_n(k\rho)\delta\hat{F}_k^n(\hat{\mu})/n_0 - \delta\hat{n}_k^e}{(T_e/T_i)\left[1 - \sum_n 2\pi \int d\hat{\mu}F_M(\hat{\mu})J_n^2(k\rho)\right] + \hat{\lambda}_D^2\hat{k}^2}. \qquad (9)$$

The polarization density formally vanishes when all cyclotron harmonics are retained: $[1 - \sum_n 2\pi \int d\hat{\mu}F_M(\hat{\mu})J_n^2(k\rho)] \rightarrow 0|_{n\rightarrow\pm\infty}$.

The radial ion particle and energy fluxes are

$$[\hat{\Gamma}, \hat{Q}^\perp] = Re\, 2\pi \int_0^\infty d\hat{\mu}$$
$$\times \sum_k\sum_n[1, (T_i/T_e)\hat{\mu}]i\hat{k}_y\delta\hat{\phi}_k^* J_n(k\rho)\delta\hat{G}_k^n(\hat{\mu})/n_0. \qquad (10)$$

C. Gyrokinetic equations

The CKinCH equation entirely recovers the gyrokinetic equation when truncated at the 0-th cyclotron harmonic. The 0-th cyclotron harmonic describes the low-frequency drift motion while other harmonics represent the high-frequency ion cyclotron motion. Keeping only the 0-th harmonic (by setting $n = n' = 0$) in Eq. (6) [or the equivalent Eq. (7)], we obtain the gyrokinetic equation

$$D\delta\hat{F}_k/D\hat{t} - i\hat{\omega}_k^d \delta\hat{G}_k = -i\hat{\omega}_*^{nT} J_0(k\rho)\delta\hat{\phi}_k n_0 F_M(\hat{\mu})$$
$$+ \sum_{k1}\hat{b}\cdot(\vec{k}_1\times\vec{k}_2)J_0(k_1\rho)\delta\hat{\phi}_{k1}\delta\hat{F}_{k2},$$
$$(11)$$

where $\delta\hat{F}_k(\hat{\mu}) = \delta\hat{G}_k(\hat{\mu}) - (T_e/T_i)\delta\hat{\phi}_k n_0 F_M(\hat{\mu})J_0(k\rho)$.

The Poisson equation of gyrokinetics is given by

$$\delta\hat{\phi}_k = \frac{2\pi\int d\hat{\mu}J_0(k\rho)\delta\hat{F}_k(\hat{\mu})/n_0 - \delta\hat{n}_k^e}{(T_e/T_i)2\pi\int d\hat{\mu}F_M(\hat{\mu})\left[1 - J_0^2(k\rho)\right] + \hat{\lambda}_D^2\hat{k}^2}, \quad (12)$$

where $2\pi\int d\hat{\mu}F_M(\hat{\mu})[1 - J_0^2(k\rho)]$ represents the ion polarization. Gyrokinetics nonlinearly conserves the incremental entropy defined as $S = 2\pi\sum_k\int_0^\infty d\hat{\mu}(\delta\hat{F}_k^*\delta\hat{F}_k)$.

The radial ion particle and energy fluxes are

$$[\hat{\Gamma}, \hat{Q}^\perp] = Re\, 2\pi\int_0^\infty d\hat{\mu}$$
$$\times \sum_k[1, (T_i/T_e)\hat{\mu}]i\hat{k}_y\delta\hat{\phi}_k^*[J_0(k\rho)\delta\hat{G}_k(\hat{\mu})/n_0].$$
$$(13)$$

D. Electron equations of motion

In this paper the electron motion equation is given by the collisional drift wave (CDW) electron model. This is essentially the Hasegawa-Wakatani[10] electron model with a grad-B drift added

$$D\delta\hat{n}_k^e/D\hat{t} + i\hat{\omega}_d^e\delta\hat{n}_k^e + \alpha_A(\delta\hat{n}_k^e - \delta\hat{\phi}_k)$$
$$= -i(\hat{\omega}_*^n - \hat{\omega}_d^e)\delta\hat{\phi}_k + \sum_{k1}\hat{b}\cdot(\vec{k}_1\times\vec{k}_2)\delta\hat{\phi}_{k1}\delta\hat{n}_{k2}^e, \quad (14)$$

where $\hat{\omega}_*^n \Rightarrow \hat{k}_y(a/L_n)$ is the density gradient drive frequency and $\hat{\omega}_d^e \Rightarrow 2\hat{k}_y(a/R)$ is the grad-B drift frequency. The factor 2 here is again used to compensate for the parallel motion curvature drive. $\alpha_A = \hat{k}_\parallel^2/[\hat{\nu}_{ei}(m_e/m_i)]$ is the CDW adiabaticity parameter used for controlling the strength of the turbulence. $\hat{k}_\parallel = a/Rq$ is the parallel wave-number and $\hat{\nu}_{ei}$ is the electron-ion collision frequency. α_A is derived from Ohm's law in the parallel direction. Large α_A leads to a lower turbulence adiabatic electron response (with only the ITG mode drive). Small α_A corresponds to a high turbulence level contributed by the resistive interchange modes. These are strongly driven at long wave length (small $\hat{k}_y$). While the overall sign of the nonlinear terms has no effect on the time average transport, it is very important that the electron $E \times B$ nonlinearity have the correct relative sign as the ion $E \times B$ nonlinearity.

TABLE I. The physics parameters of the standard case.

a/L_n	a/L_{Ti}	α_A	a/R	μ_{LK}	μ_{HK}	$\Omega*$	$\hat{\lambda}_D$	C_{DW}
4.00	4.00	1.0	0.3	0.05	0.3	10	0.1	1

III. SIMULATION RESULTS

A. Standard test case with stable ion cyclotron (IC) modes

The parameters of the standard case are listed in Tables I and II. All calculations in this paper are performed using these parameters unless specified otherwise. The grid convergences were tested in Ref. 6. The number of modes N_k saturates after $N_k = 17 \times 17 = 289$ with $N_k = 21 \times 21 = 441$ chosen for the standard case. μ-grid number N_μ saturates after $N_\mu = 11$ with $N_\mu = 21$ chosen for the standard case. Number of harmonics $(2N_\alpha - 1)$ of gyro-phase motion saturates after 7 with 9 used for the standard case. The standard case parameters for CHinCH simulations below are the same as those in Ref. 6 for the CHinFH simulations.

Figure 1 shows the cyclokinetic linear growth rate $\hat{\gamma}$ of the leading low-frequency mode and the corresponding frequency $\hat{\omega}$ using the eigenvalue solver of rCYCLO.[6] The frequency and growth rate of low-frequency drift modes of CKinCH are identical to those of gyrokinetics (GK) as well as CKinFH. The undamped leading low-frequency drift waves are unstable while the undamped high-frequency ion cyclotron modes are marginally stable. The addition of the low-k damping $\mu_{LK}/\hat{k}^2$ (high-k damping $\mu_{HK}\hat{k}^4$) stabilizes the low-k (high-k) modes providing a sink of incremental entropy. The nonlinear terms transfer the incremental entropy from the unstable source modes to the stable sink modes in k space.

Fig. 2 illustrates the nonlinear saturation processes in the time initial evolution of the standard case. The time average of the energy diffusivity over the saturated time period is $\hat{\chi}^{GK} = 13.1 \pm 0.1$ for gyrokinetics, and $\hat{\chi}^{CK} = 3.18 \pm 0.07$ for cyclokinetics, respectively. The corresponding particle diffusivity is $\hat{D}^{GK} = 9.8 \pm 0.4$ for gyrokinetics, and $\hat{D}^{CK} = 2.82 \pm 0.07$ for cyclokinetics, respectively. The time step of the standard case is $\Delta\hat{t} = 0.001\, a/c_s$ for gyrokinetics, and $\Delta\hat{t} = 0.0005\, a/c_s$ for cyclokinetics, respectively. The time step is chosen to conserve the incremental entropy with the error less than a percent when all the linear terms are removed. In general the time step should be smaller when $\Omega*$ is higher, e.g., $\Delta\hat{t} = 0.00005\, a/c_s$ is chosen for the cyclokinetic case at $\Omega* = 100$. Fig. 3 shows the frequency spectrum of $\hat{\chi}^{CK}$ and $|\delta\hat{\phi}|^2$ of CKinCH standard case during the saturated time period, which clearly shows the low-frequency drift-wave modes and the four harmonics of high-frequency ion cyclotron modes with $\hat{\omega}$ close to ± 10 and ± 20. The linearly damped high-frequency IC modes are nonlinearly driven by the low-frequency unstable drift modes

TABLE II. The grid parameters of the standard case.

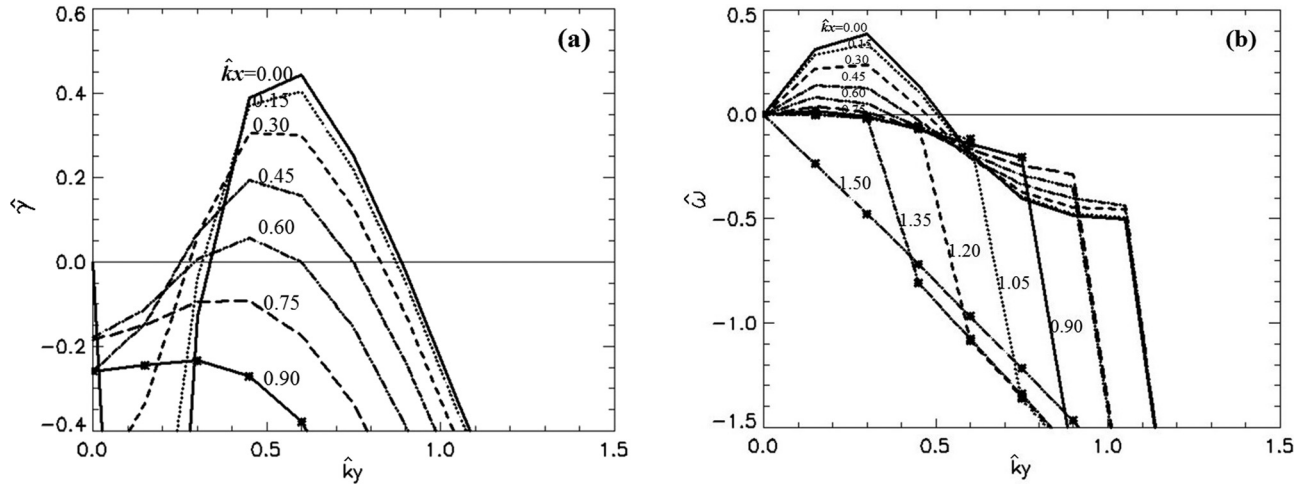| N_k	$\hat{k}_x^{max}(= \hat{k}_y^{max})$	N_μ	N_α
21×21	1.5	21	5

FIG. 1. (a) The linear growth rate $\hat{\gamma}$, and (b) frequency $\hat{\omega}$ spectrums of the CKinCH standard case solved by the eigenvalue solver of rCYCLO.[6] Only the $k_x > 0$ and $k_y > 0$ modes are presented.
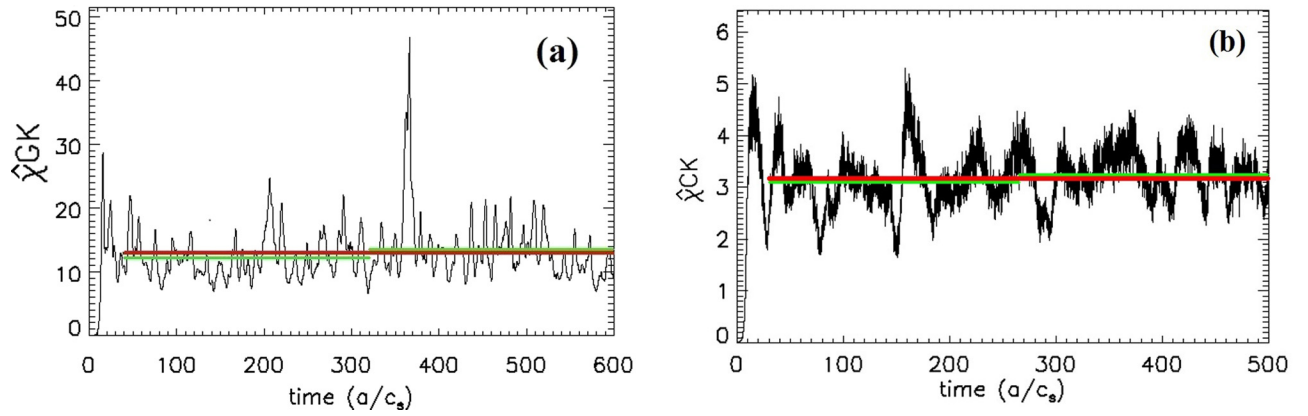

FIG. 2. The time evolution of turbulent energy diffusivity of (a) GK and (b) CKinCH standard case. The average energy diffusivity over the saturated period of time is (a) 13.1 ± 0.1 for GK, (b) 3.18 ± 0.07 for CKinCH. The red and green lines represent the average over the all saturated time and the half period of saturated time, respectively.
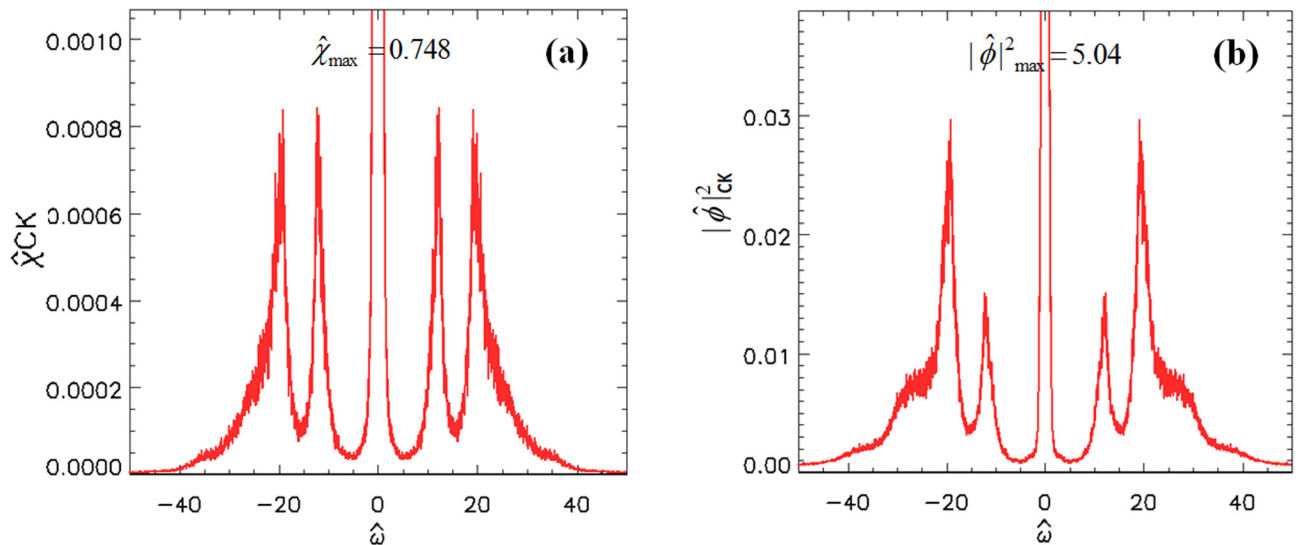

FIG. 3. The frequency spectrum for the CKinCH standard case during the saturated time. (a) $\hat{\chi}^{CK}$ versus $\hat{\omega}$, and (b) $|\hat{\phi}|^2$ versus $\hat{\omega}$. The drift-wave modes ($\hat{\omega}$ close to 0) and the four harmonics of the high-frequency IC modes ($\hat{\omega}$ close to ± 10, and ± 20) are clearly shown.
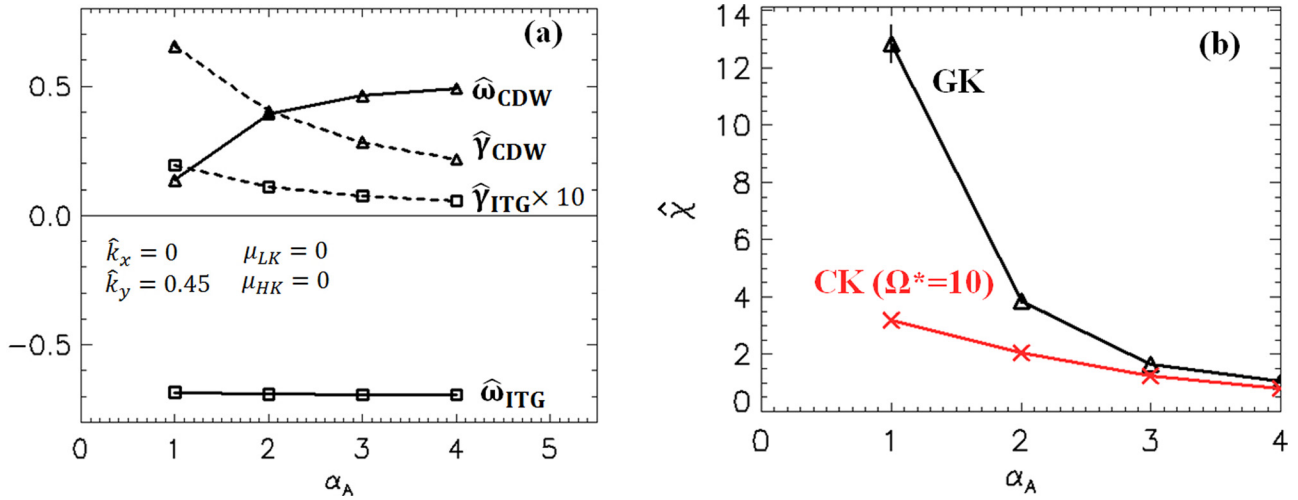
FIG. 4. (a) The low-frequency drift mode growth rate $\hat{\gamma}$ and frequency $\hat{\omega}$ of the standard CKinCH case versus α_A at the fixed point $\hat{k}_x = 0$ and $\hat{k}_y = 0.45$ with damping $\mu_{LK} = 0$ and $\mu_{HK} = 0$. The frequency of ITG modes $\hat{\omega}_{ITG}$ is negative and the corresponding growth rate $\hat{\gamma}_{ITG}$ is small [$\hat{\gamma}_{ITG}$ has been multiplied by 10 in (a)]. The CDW modes are the most unstable modes and their frequency $\hat{\omega}_{CDW}$ is positive. CDW modes will switch to more unstable resistive-g modes with the smaller α_A. (b) The energy diffusivity of gyrokinetics $\hat{\chi}^{GK}$ and cyclokinetics $\hat{\chi}^{CK}$ at $\Omega^* = 10$ versus α_A.

which satisfy the wave-wave coupling condition. The low-frequency unstable drift modes account for most (e.g., 87% within $|\hat{\omega}| \leq 2$) of the transport.

The two kinds of low-frequency drift modes, ion temperature gradient (ITG) modes, and CDW modes are described in Fig. 4(a). It shows the standard CKinCH case and fixes $\hat{k}_x = 0$ *and* $\hat{k}_y = 0.45$ with damping $\mu_{LK} = 0$ and $\mu_{HK} = 0$. The negative frequency ITG modes are slightly unstable and nearly independent of α_A [the growth rate of ITG modes $\hat{\gamma}_{ITG}$ has been multiplied by 10 in Fig. 4(a)]. The positive frequency CDW modes are the most unstable modes. The low-collisional (large α_A) electron modes approach the adiabatic limit, while the highly collisional (small α_A) electron modes transform to the more unstable resistive-g modes at very small α_A. Since the growth rates of the CDW modes decrease much faster than the ITG modes when $\hat{k}_x$ and $\hat{k}_y$ increase, the dominant modes will switch from CDW modes to ITG modes when either $\hat{k}_x$ or $\hat{k}_y$ increases larger than 1.0. The jumps in frequency spectrum

shown in Fig. 1(b) illustrate this mode switch phenomenon. The nonlinear turbulent transport level of gyrokinetics increases faster than cyclokinetics with decreasing α_A as illustrated in Fig. 4(b).

B. Gyrokinetics breaks down at low Ω^* and high turbulence levels but recovers cyclokinetics at high Ω^* and low turbulence levels

The linear growth rates and frequencies of gyrokinetics recover the growth rates and frequencies of cyclokinetics at low-frequency regime as shown in Figs. 5(a) and 5(b). The cyclokinetic IC modes are stable as shown in Fig. 5(a). In the cyclokinetic simulations, the turbulence is drained from the unstable drift modes to the stable IC modes. Fig. 5(b) illustrates the frequency of $n = \pm 1$ harmonics are around ∓ 10. The IC mode frequency deviates from -10 at high k is caused by the linear coupling to the low-frequency drift modes.
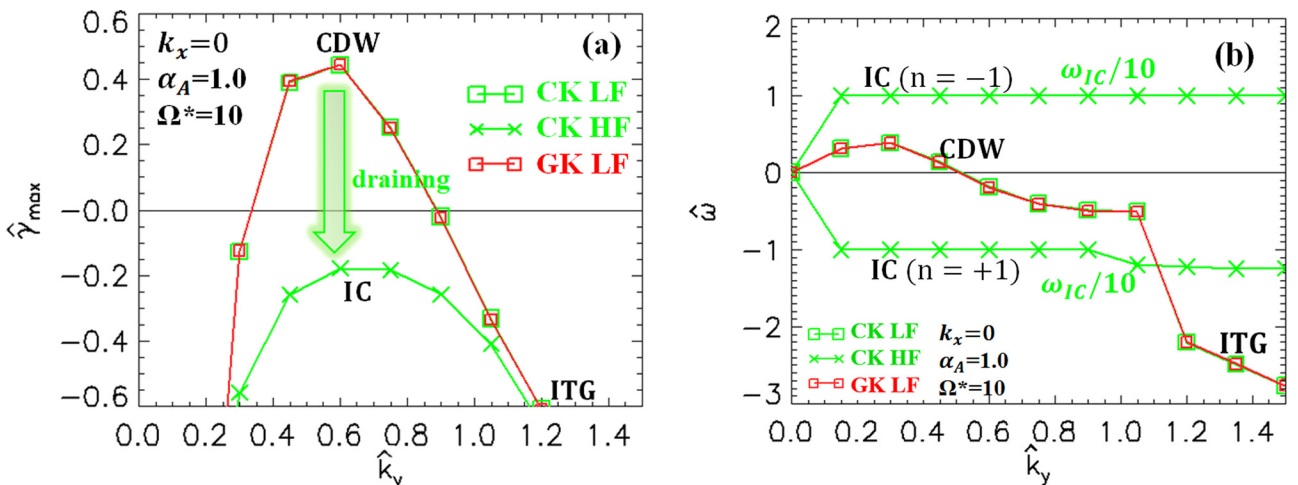

FIG. 5. (a) Linear growth rates and (b) the corresponding frequencies of GK, CKinCH low-frequency (LF) modes and CKinCH high-frequency (HF) modes at the fixed $\hat{k}_x = 0$ of standard case. The frequencies of IC $n = -1, +1$ harmonics are divided by 10 in (b).
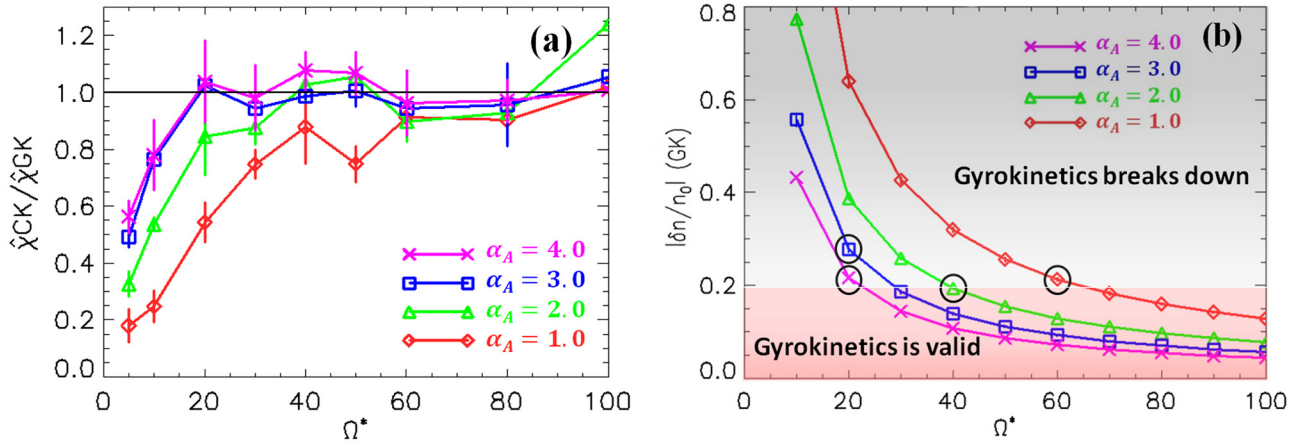
FIG. 6. (a) The energy diffusivity ratio of CKinCH over gyrokinetics versus Ω^*. The transport level of gyrokinetics recovers CKinCH at high-Ω^* values and low turbulence levels. Cyclokinetic transport level is lower than gyrokinetics at low-Ω^* values and high turbulence levels. (b) The time average of turbulence level $|\delta n/n_0|$ versus Ω^*. The black circles mark where gyrokinetics starts to break down, which indicates that gyrokinetics starts to break down when $|\delta n/n_0| > 20\%$.

At sufficiently large Ω^* and sufficiently low turbulence level, the nonlinear gyrokinetic simulations have recovered the cyclokinetic transport levels as shown in Fig. 6(a). The transport level of cyclokinetics is lower than the gyrokinetic transport at low-Ω^* values. The lower cyclokinetic transport level results from the turbulence being drained to the less unstable IC modes [shown in Fig. 5(a)]. The cyclokinetic nonlinear coupling is enhanced at low velocity by the $1/\hat{v}_\perp$ factor in Eqs. (6) and (7). Fig. 6(a) is *nearly* identical to Fig. 9 of Ref. 6 obtained from CKinFH simulations with the same standard grid parameters, which verified that the numerical simulations of CKinCH recovered both the linear and nonlinear simulations of CKinFH in Ref. 6. Fig. 6(b) shows the time average of the turbulence level $|\delta n/n_0|$ versus Ω^*. In gyrokinetic simulations $|\delta n/n_0|_{GK} \propto 1/\Omega^* = \rho^*$. Fig. 6(b) indicates that gyrokinetics starts to break down when $|\delta n/n_0|$ exceeds 20% marked by the black circles. The low-frequency gyrokinetic approximation requires that the nonlinear perturbed $E \times B$ frequency $|\omega_{NL}/\Omega| = (1/N_k)$

$\sum_k |\vec{k} \cdot \delta\vec{v}_E|/\Omega = (1/N_k)\sum_k |(\vec{k}\rho) \cdot (\delta\vec{v}_E/v_i^{th})| = (\rho^*/N_k)$ $\sum_k |Re[(-i)\sum_{k1}\vec{k} \cdot \vec{k}_1 \times \hat{b}\delta\hat{\phi}_{k1}]|$ is small. It is also proportional to ρ^* like $|\delta n/n_0|$. For the examples in Fig. 6, $\omega_{NL}/\Omega \sim 2.3|\delta n/n_0|$ corresponds to the gyrokinetic breakdown at $|\omega_{NL}/\Omega| > 45\%$.

The cyclokinetic small $\Omega^* = 1/\rho^*$ stabilizing effect on gyrokinetics from coupling to stable high-frequency modes is analogous to the global gyrokinetic large ρ^* stabilizing effect from nonlocal turbulence spreading (NTS).[7] Both L-mode and H-mode DIII-D simulations[8] with the GYRO code show that the NTS mechanism breaking gyroBohm scaling is due to the nonlocal drainage of turbulence from the unstable radii and spreading to the stable (or less unstable) radii. At larger ρ^* where the small "local" eddies become the large "global" eddies, there is a transition from gyroBohm scaling $\chi_{gB} = (c_s/a)\rho_s^2$ to Bohm scaling $\chi_B = \chi_{gB}/\rho^* = \chi_{gB}\Omega^*$. At smaller Ω^*, cyclokinetics transitions in a similar way. The turbulence is drained in the frequency space rather than
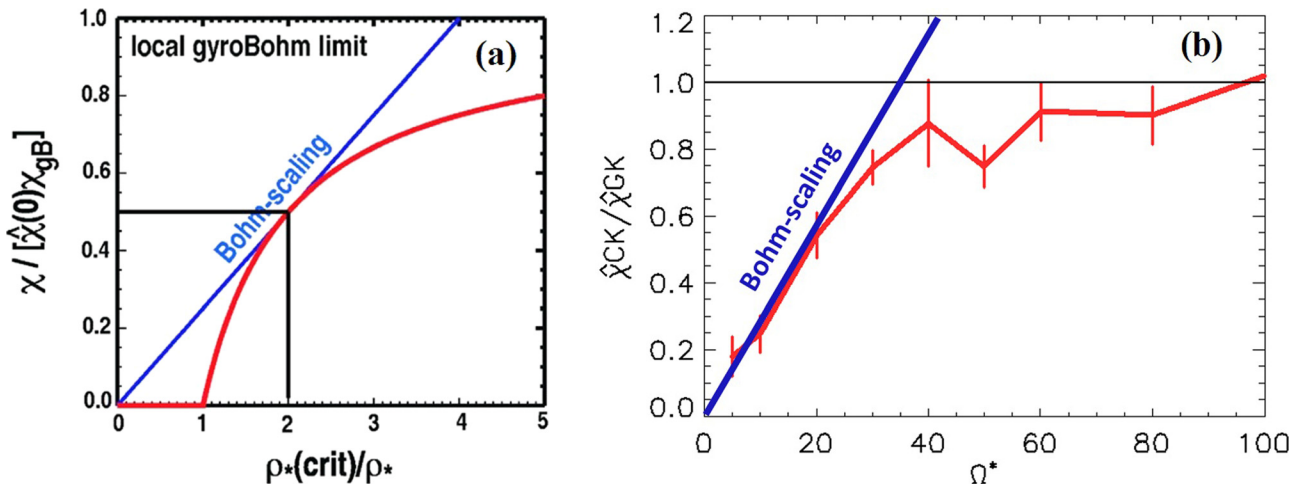

FIG. 7. (a) is from Ref. 8 which shows the rule for breaking gyroBohm scaling by the NTS mechanism. Global gyrokinetic energy diffusivity normalized by gyroBohm level at $\rho^* \Rightarrow 0$ vs ρ^*_{crit}/ρ^*. Reprinted with permission from Phys. Plasmas **13**, 072304 (2006). Copyright 2006 AIP Publishing LLC. (b) Local cyclokinetic energy diffusivity normalized by gyrokinetic diffusivity vs Ω^*, which indicates that the cyclokinetics has the similar rule for breaking gyroBohm scaling by nonlocal turbulence spreading in frequency space.

radial space from the unstable low-frequency domain and spreads into the less unstable high-frequency domain. The NTS paradigm for breaking the gyroBohm scaling in the unstable regions $\chi = \hat{\chi}(0)\chi_{gB}(1 - \rho^*/\rho^*_{crit})$ is represented by Fig. 7(a) taken from Ref. 8. The cyclokinetic high-frequency stabilization can be written analogously $\hat{\chi}^{CK} = \hat{\chi}^{GK}(1 - \Omega^*_{crit}/\Omega^*)$ as represented in Fig. 7(b). The Ω^*_{crit} increases when the turbulence level increases as shown in Fig. 6(a). Furthermore, in the stable (or less unstable) region, where the local gyroBohm diffusivity is expected to be smaller, the radially nonlocal NTS mechanism can be represented by $\chi = \hat{\chi}(0)\chi_{gB}(1 + \rho^*/\rho^*_{crit})$.[8] It has a contribution from super-gyroBohm to gyroBohm χ_{gB}. Thus, the transport level is higher than the local gyroBohm because the turbulence spreads into this less unstable radii from a more unstable radii. This suggests that if the cyclokinetic high-frequency IC modes are driven sufficiently unstable, it might be reasonable to expect that $\hat{\chi}^{CK} = \hat{\chi}^{GK}(1 + \Omega^*_{crit}/\Omega^*)$ with the cyclokinetic low-frequency mode transport level possibly higher than gyrokinetics, because the direction of draining and spreading might be reversed.

C. Cyclokinetic simulations with unstable ion cyclotron (IC) modes

In order to obtain the unstable high-frequency IC modes, we add an artificial driving term $n\gamma_{IC}H(\hat{k}_y)\delta\hat{F}^n_k$ to the $n = -1$ and $+1$ harmonics of Eq. (6) [or equivalently Eq. (7)]. $H(\hat{k}_y) = -1.778\hat{k}_y^2 + 2.667|\hat{k}_y|$ is a model function with the maximum value $H(\hat{k}_y)|_{max} = 1.0$ at $\hat{k}_y = 0.75$. γ_{IC} is a constant and represents the maximum driving rate added on the IC modes. Thus, we can drive the high-frequency IC modes unstable without affecting the low-frequency drift modes as shown in Fig. 8. The same artificial damping rates $\mu_{HK}\hat{k}^4$ and $\mu_{LK}/\hat{k}^2$ of drift wave modes are added to the IC modes. We have verified that the cyclokinetic transport level is insensitive to these damping rates of IC modes as long as IC modes are less unstable than low-frequency drift modes.

Figs. 9(a) and 9(b) describe the γ_{IC} scan of the energy diffusivity ratio $\hat{\chi}^{CK}/\hat{\chi}^{GK}$ and the electrostatic energy ratio
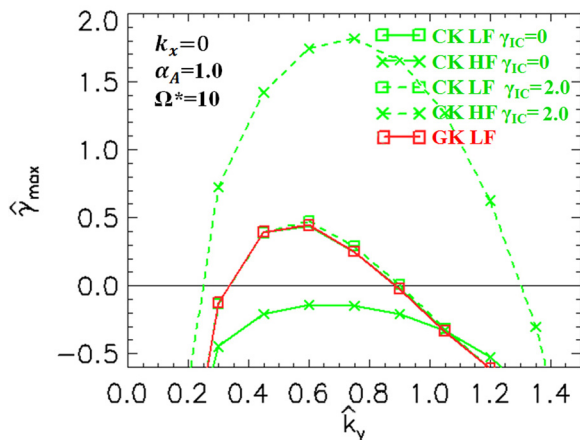

FIG. 8. Linear growth rates of GK, CKinCH low-frequency (LF) modes and CKinCH high-frequency (HF) modes with $\gamma_{IC} = 0$ and 2.0 at the fixed $\hat{k}_x = 0$ of standard case.

$\hat{E}^{CK}/\hat{E}^{GK}$ at $\Omega^* = 10$. The turbulent electrostatic energy is defined as $\hat{E} = (1/2)\sum_k \hat{k}^2 \delta\hat{\phi}^*_k \delta\hat{\phi}_k$. $\hat{\chi}^{GK}$ and $\hat{E}^{GK}$ are constant with respect to γ_{IC}/Ω^*. There are two different regimes for each curve and a jump of $\hat{\chi}^{CK}/\hat{\chi}^{GK}$ between the two regimes but no jump of $\hat{E}^{CK}/\hat{E}^{GK}$ (with minor exception at $\alpha_A = 4$). Notice that the $\hat{\chi}^{CK}$ can be driven higher than $\hat{\chi}^{GK}$.

In order to illustrate the jump, we give more details of the $\alpha_A = 2$ case in Figs. 9(a) and 9(b): Figs. 9(c) and 9(d) show the γ_{IC} scan of the ratio $\hat{\chi}^{CK}/\hat{\chi}^{GK}$ and $\hat{E}^{CK}/\hat{E}^{GK}$ contributed by high-frequency modes and low-frequency modes, respectively. The jump is obtained (at all Ω^*) when the maximum high-frequency (HF) driving rate is about twice the maximum low-frequency (LF) driving rate, e.g., the jump of the $\alpha_A = 2$ curve occurs when γ_{IC}/Ω^* is between 0.078 and 0.085 shown by Fig. 9(c) where LF driving rate is 0.44 and HF driving rate is from 0.78 to 0.85. Just before the jump (γ_{IC}/Ω^* smaller than 0.078), about 90% transport is generated by the low-frequency ($|\hat{\omega}| \leq 2$) modes and about 10% from the high-frequency ($|\hat{\omega}| > 2$) modes. Then the transport from high-frequency modes jumps up to 90%, and the transport from low-frequency modes falls down to 10% at the jump regime of γ_{IC}/Ω^* from 0.078 to 0.085 in Fig. 9(c). After the jump (γ_{IC}/Ω^* larger than 0.085), $\hat{\chi}^{CK}$ increases quite rapidly with increasing γ_{IC} in the dominantly high-frequency mode regime. Before the jump, the turbulence is drained from the unstable low-frequency domain and spreads into the less unstable high-frequency domain. After the jump, the turbulence is drained from the more unstable high-frequency domain and spreads into the less unstable low-frequency domain. The jump corresponds to where the direction of draining and spreading is reversed. The rapid increase of cyclokinetic transport after the jump in Fig. 9(c) results from the high-frequency IC modes, which are directly driven by γ_{IC}. The high-frequency IC modes produce more than 90% transport in this regime. When γ_{IC} increases to a large value, the high-frequency IC modes are much more unstable than the low-frequency drift modes. The transport of cyclokinetics will get much larger than gyrokinetics, e.g., 2.3 times larger with $\gamma_{IC}/\Omega^* = 0.4$ and $\alpha_A = 2$. More importantly the high-frequency component of $\hat{\chi}^{CK}$ can exceed $\hat{\chi}^{GK}$, but the low-frequency component of $\hat{\chi}^{CK}$, which is associated with the "short-fall," is still much smaller than $\hat{\chi}^{GK}$ as shown by Fig. 9(c). We only focus on the transport of low-frequency component in this work, since only the low-frequency turbulence is measured in experiments.[2]

To explain the jump down of the high-frequency cyclokinetic transport, we note that from Eq. (10) and the linear part of Eq. (14) we know that the diffusivity is proportional to diffusivity correlation phase factor: $\hat{\chi} \propto \hat{D} \propto \sum_k \hat{E}\, C(\hat{\omega})$. The phase factor $C(\hat{\omega})$ is a strong function of frequency $C(\hat{\omega}) = (\hat{k}_y/\hat{k}^2)[\alpha_A(\hat{\omega}^n_* - \hat{\omega}) + \hat{\gamma}(\hat{\omega}^n_* - \hat{\omega}^e_d)]/[(\alpha_A + \hat{\gamma})^2 + (\hat{\omega} - \hat{\omega}^e_d)^2]$, which is roughly proportional to $1/\hat{\omega}$ when $\hat{\omega}$ is large. Thus, the low-frequency component has a big phase factor, and the high-frequency component has a small phase factor. When the direction of draining and spreading is reversed, $\hat{E}^{CK}$ is unchanged in total but redistributed from low-frequency modes to high-frequency
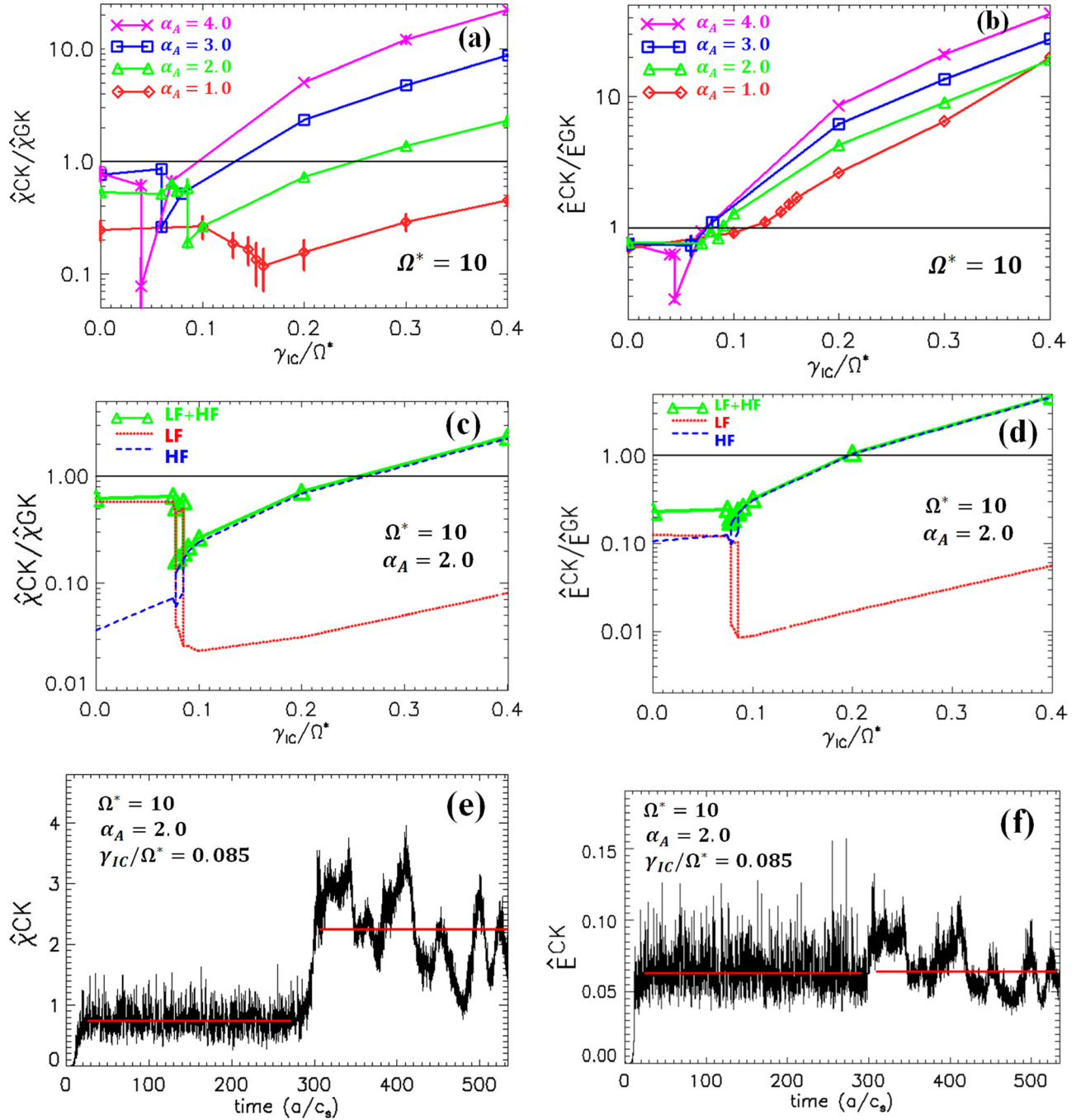
FIG. 9. (a) and (b) show the energy diffusivity ratio $\hat{\chi}^{CK}/\hat{\chi}^{GK}$ and the electrostatic energy ratio $\hat{E}^{CK}/\hat{E}^{GK}$ of CKinCH over gyrokinetics versus γ_{IC}/Ω^* at $\Omega^* = 10$. There are two different regimes for each curve and a jump of $\hat{\chi}^{CK}/\hat{\chi}^{GK}$ between the two regimes but no jump of $\hat{E}^{CK}/\hat{E}^{GK}$ with minor exception at $\alpha_A = 4$. $\hat{\chi}^{GK}$ and $\hat{E}^{GK}$ are constant with respect to γ_{IC}/Ω^*. (b) and (d) describe the high-frequency component (by the blue dashed curve) and low-frequency component (by the red dot curve) of $\hat{\chi}^{CK}/\hat{\chi}^{GK}$ and $\hat{E}^{CK}/\hat{E}^{GK}$ versus γ_{IC}/Ω^* at $\alpha_A = 2$ and $\Omega^* = 10$. The green curves represent the summation of low-frequency and high-frequency components. $\gamma_{IC}/\Omega^* = 0$–0.078 are the dominantly low-frequency drift mode regimes. $\gamma_{IC}/\Omega^* = 0.078$–0.085 correspond to the jump regimes. $\gamma_{IC}/\Omega^* = 0.085$–0.4 are the dominantly high-frequency IC mode regimes. The high-frequency component of $\hat{\chi}^{CK}$ can exceed $\hat{\chi}^{GK}$, but the low-frequency component cannot. (e) and (f) illustrate $\hat{\chi}^{CK}$ and $\hat{E}^{CK}$ versus time at $\gamma_{IC}/\Omega^* = 0.085$, $\alpha_A = 2$, and $\Omega^* = 10$. The turbulence saturates to two steady states, respectively, during time period $21 \sim 270\, a/c_s$ and $312 \sim 534\, a/c_s$. The red lines represent the time average of each state. There is a jump of $\hat{\chi}^{CK}$, while there is no jump of $\hat{E}^{CK}$.

modes. When the energy is transferred from low-frequency modes to high-frequency modes, the cyclokinetic transport level $\hat{\chi}^{CK}$ will jump down.

Bifurcated turbulent transport states are always found in the jump regimes for $\alpha_A = 2, 3, 4$ (but not for $\alpha_A = 1$). These two nonlinear cyclokinetic saturated states are associated with two different basins of attraction, which could be considered analogous to Lorenz attractors.[11] Fig. 9(e) illustrates

that the turbulence firstly saturates to a low-level state, where the high-frequency modes occupy 85% of the transport during the time period $21 \sim 270\, a/c_s$. Then the turbulence level jumps and saturates to a higher level state in the time period $312 \sim 534\, a/c_s$, where the low-frequency modes occupy 85% of the transport. Fig. 9(f) shows that the cyclokinetic electrostatic energy $\hat{E}^{CK}$ saturates to the same two states but without a jump in total.
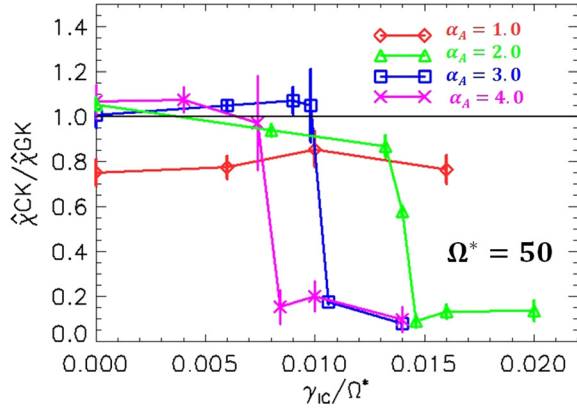
FIG. 10. The energy diffusivity ratio of CKinCH over gyrokinetics versus γ_{IC}/Ω^* at $\Omega^* = 50$.

From Eq. (8) of Drummond and Rosenbluth early work on current drift driven ion cyclotron modes,[12] we have some idea of a physically reasonable IC drive rate: $\hat{\gamma}/\Omega^* \cong 0.3(T_e/T_i)v_D/v_e^{th}$. v_e^{th} is the electron thermal velocity. v_D is the electron current drift velocity relative to the stationary ions. A maximal value of $v_D/v_i^{th} = 5$ corresponds to a growth rate of $\hat{\gamma}/\Omega^* = 0.025$ (for $T_e = T_i$ and deuterium). This growth rate is not large enough to drive either LF or HF cyclokinetic turbulence level higher than gyrokinetics at $\Omega^* = 10$ shown by Fig. 9(a). $\gamma_{IC}/\Omega^* = 0.025$ is even well below the jump regime between 0.078 and 0.085.

For a more physically relevant ion cyclotron frequency value $\Omega^* = 50$, the jump happens again as shown by Fig. 10 when the maximum high-frequency driving rate is about twice the maximum low-frequency driving rate. However, the IC driving rate $\hat{\gamma}/\Omega^* = 0.025$ is still not large enough to drive either LF or HF cyclokinetic turbulent transport higher than gyrokinetics. Thus, the L-mode near edge "short-fall" is not due to the nonlinear coupling between low-frequency drift motion and high-frequency ion cyclotron motion. At large Ω^* value ($\Omega^* \geq 50$) the high-frequency IC modes are decoupled from the low-frequency drift modes. The nonlinear interaction is no longer strong enough to saturate the very unstable IC modes for $\gamma_{IC}/\Omega^* > 0.02$.

IV. CONCLUSIONS

We have done the first nonlinear cyclokinetic (in the cyclotron harmonic representation) simulations to compare with the less fundamental gyrokinetic simulations in this paper.

We find that at sufficiently large Ω^* and sufficiently low turbulence levels, the nonlinear gyrokinetic simulations have recovered the cyclokinetic transport levels as required. This result is one of the most important verifications of cyclokinetic simulations. With stable IC modes, the transport level of cyclokinetics is lower than the transport level of gyrokinetics at low-Ω^* values and high turbulence levels. Gyrokinetics starts to break down when turbulence level $|\delta n/n_0| > 20\%$. The transport level of cyclokinetics is lower than that of gyrokinetics because the turbulence is drained to the less unstable IC modes.

The cyclokinetic simulations with sufficiently unstable IC modes offer the possibility that cyclokinetic transport

could be driven higher than the gyrokinetics. However, in these cases only the high-frequency component of cyclokinetic transport level was found to exceed the gyrokinetic transport level at sufficient low $\Omega^* \sim 10$. Even for this low Ω^*, the low-frequency component of the cyclokinetic transport and turbulence level did not exceed that of gyrokinetics. Furthermore, at higher and more physically relevant $\Omega^* \geq 50$ values with more physically realistic IC driving rates, the low-frequency component of the cyclokinetic turbulence level and transport did not exceed that of gyrokinetics. Thus, the cyclokinetic simulations do not account for the so-called "L-mode near edge short fall" seen in some low-frequency gyrokinetic transport and turbulence simulations. Although the highly driven IC mode low-Ω^* simulations are not physically relevant, they were found to provide a perhaps unique example of bifurcated turbulent transport states.

Additional simulations (not shown in this work) with unstable ITG modes, stable IC modes, and adiabatic electrons found very similar results, namely, that cyclokinetic transport is always smaller than gyrokinetic transport.

APPENDIX: CYCLOKINETIC EQUATIONS IN FOURIER HARMONIC FORM

Ref. 6 presented the formulas and simulations of CKinFH. For the convenience of readers, we list the equations here. After straightforwardly expanding $\delta\hat{f}_k(\hat{\mu}, \alpha)$ with discrete Fourier harmonics $\delta\hat{f}_k(\hat{\mu}, \alpha) = \sum_{n=-N_\alpha+1}^{n=N_\alpha-1} \delta\hat{F}_k^n(\hat{\mu}) \exp(in\alpha)$, we obtain the CKinFH equation

$$D\delta\hat{F}_k^n/D\hat{t} - i\hat{\omega}_k^d\delta\hat{G}_k^n + i(\hat{v}_\perp\hat{k}/2)\Omega_*[\exp(-i\beta)\delta\hat{G}_k^{n-1}$$
$$+ \exp(+i\beta)\delta\hat{G}_k^{n+1}] - \Omega_* in\hat{G}_k^n$$
$$= -i\hat{\omega}_{*k}^{nT}\delta\hat{\phi}_k n_0 F_M(\hat{\mu})\delta_0^n + {}^{NL}S(\hat{k}, \hat{\mu}, n), \quad (A1)$$

where $\delta\hat{G}_k^n = \delta\hat{F}_k^n + (T_e/T_i)\delta\hat{\phi}_k n_0 F_M(\hat{\mu})\delta_0^n$ with $\delta_0^n = [0, 1]$ corresponding to $[n \neq 0, n = 0]$, respectively. The perturbed distribution functions are linearly coupled and satisfy the reality condition $\delta\hat{F}_{-k}^{-n} = [\delta\hat{F}_k^n]^*$. ${}^{NL}S(\hat{k}, \hat{\mu}, n)$ represents the nonlinear dynamics, for which the conservative form is

$${}^{NL}_{Con}S(\hat{k}, \hat{\mu}, n) = \partial_{\hat{\mu}}\sum_{k1}(T_e/T_i)\delta\hat{\phi}_{k1}i(\hat{v}_\perp\hat{k}_1/2)$$
$$\times [\exp(-i\beta_1)\delta\hat{F}_{k2}^{n-1} + \exp(+i\beta_1)\delta\hat{F}_{k2}^{n+1}]$$
$$-\sum_{k1}\delta\hat{\phi}_{k1}i\hat{k}_1/(2\hat{v}_\perp)n[\exp(-i\beta_1)\delta\hat{F}_{k2}^{n-1}$$
$$- \exp(+i\beta_1)\delta\hat{F}_{k2}^{n+1}], \quad (A2)$$

and the non-conservative form is

$$
\begin{aligned}
{}^{NL}_{NCon}S(\hat{k}, \hat{\mu}, n) = &\sum_{k1} (T_e/T_i)\delta\hat{\phi}_{k1} i(\hat{v}_\perp \hat{k}_1/2) \\
&\times [\exp(-i\beta_1)\partial_{\hat{\mu}}\delta\hat{F}^{n-1}_{k2} + \exp(+i\beta_1)\partial_{\hat{\mu}}\delta\hat{F}^{n+1}_{k2}] \\
&- \sum_{k1} \delta\hat{\phi}_{k1} i\hat{k}_1 [\exp(-i\beta_1)(n-1)\delta\hat{F}^{n-1}_{k2} \\
&- \exp(+i\beta_1)(n+1)\delta\hat{F}^{n+1}_{k2}]/(2\hat{v}_\perp). \quad (A3)
\end{aligned}
$$

The Poisson equation for CKinFH is given as

$$
(\hat{\lambda}_D^2 \hat{k}^2)\delta\hat{\phi}_k = 2\pi \int d\hat{\mu}\,\delta\hat{F}^0_k(\hat{\mu})/n_0 - \delta\hat{n}^e_k. \quad (A4)
$$

The particle and energy fluxes are given by

$$
[\hat{\Gamma}, \hat{Q}^\perp] = Re\, 2\pi \int_0^\infty d\hat{\mu} \sum_k [1, (T_i/T_e)\hat{\mu}] i\hat{k}_y \delta\hat{\phi}^*_k [\delta\hat{G}^0_k(\hat{\mu})/n_0]. \quad (A5)
$$

Only the zero-th Fourier harmonic $\delta\hat{F}^0_k$ contributes to the electrostatic potential and transport.

[1] J. Candy and R. E. Waltz, Phys. Rev. Lett. **91**, 045001 (2003).
[2] C. Holland, A. E. White, G. R. Mckee, M. W. Shafer, J. Candy, R. E. Waltz, L. Schmitz, and G. R. Tynan, Phys. Plasmas **16**, 052301 (2009).
[3] R. E. Waltz, "Search for the missing L-mode edge transport and possible breakdown of gyrokinetics," BAPS Ser. II **57**(12), 105 (2012).
[4] R. E. Waltz and Zhao Deng, Phys. Plasmas **20**, 012507 (2013).
[5] R. D. Hazeltine and J. D. Meiss, *Plasma Confinement* (Addison-Wesley, 1992).
[6] Zhao Deng and R. E. Waltz, "Numerical methods and nonlinear simulations of cyclokinetics" (submitted).
[7] Z. Lin, S. Ethier, T. S. Halm, and W. Tang, Phys. Rev. Lett. **88**, 195004 (2002).
[8] R. E. Waltz, J. Candy, and C. C. Petty, Phys. Plasmas **13**, 072304 (2006).
[9] J. Candy and R. E. Waltz, Phys. Plasmas **13**, 032310 (2006).
[10] A. Hasegawa and M. Wakatani, Phys. Rev. Lett. **50**, 682 (1983).
[11] E. N. Lorenz, J. Atmos. Sci. **20**, 130 (1963).
[12] W. E. Drummond and M. N. Rosenbluth, Phys. Fluids **5**, 1507 (1962).